processes

MDPI

Article

A Novel Control Algorithm of the Air Supply Subsystem: Based on Dynamic Modeling of Proton Exchange Membrane Fuel Cell

Pengyu Wang [1,2], Yangyang Ma [2], Jianhua Li [2,*], Yukun Gao [2], Yunrui Zhang [2] and Denghui Ma [2]

[1] State Key Laboratory of Automotive Simulation and Control, Jilin University, Changchun 130012, China; wangpy@jlu.edu.cn
[2] College of Automotive Engineering, Jilin University, Changchun 130012, China; yyma20@mails.jlu.edu.cn (Y.M.); gaoyk19@163.com (Y.G.); yunrui21@mails.jlu.edu.cn (Y.Z.); madh21@mails.jlu.edu.cn (D.M.)
* Correspondence: ljh_lotus@126.com

Abstract: In this paper, a novel second-order active disturbance rejection control (2-ADRC) algorithm is proposed to optimize the control of the air supply subsystem for Proton Exchange Membrane Fuel Cell (PEMFC). To improve the optimal control effect of the air supply subsystem for PEMFC, the modeling theory of the air supply subsystem considering dynamic characteristics of the PEMFC system is first studied, and the dynamic Simulink model of the PEMFC system is established and verified. Then, the optimal oxygen excess ratio (OER) parameters under different load currents are obtained, and the optimal OER parameters are also used as the OER control reference for the designed algorithms. In addition, a 2-ADRC algorithm is designed and proposed to make the actual OER parameters close to the optimal OER in real time. Furthermore, compared with PID and MPC algorithms, the 2-ADRC algorithm can comprehensively consider the two parameters of mass flow and pressure ratio to make the compressor work in the high-efficiency zone and improve the net power and efficiency of the PEMFC system.

Keywords: oxygen excess ratio; dynamic modeling; proton exchange membrane fuel cell; control algorithm

Citation: Wang, P.; Ma, Y.; Li, J.; Gao, Y.; Zhang, Y.; Ma, D. A Novel Control Algorithm of the Air Supply Subsystem: Based on Dynamic Modeling of Proton Exchange Membrane Fuel Cell. *Processes* **2022**, *10*, 1499. https://doi.org/10.3390/pr10081499

Academic Editor: Alfredo Iranzo

Received: 24 June 2022
Accepted: 26 July 2022
Published: 29 July 2022

1. Introduction

Fuel cell vehicles (FCVs) have the advantages of zero emissions during driving, no anxiety in driving mileage and smooth operation without noise [1]. FCVs have gradually become the mainstream development direction of new energy vehicles, attracting the attention of governments and research institutes around the world. As the main component and key technology of FCVs [2], the selection of fuel cell system (FCS) is crucial to improve the comprehensive performance of FCVs. Proton exchange membrane fuel cell (PEMFC) has been considered as the most suitable energy source for FCVs because of its superior performance such as high efficiency, zero emission and modularity [3].

PEMFC is composed of a fuel cell stack, air supply subsystem, hydrogen supply subsystem and cooling subsystem, etc. [4]. The air supply subsystem is very significant to the dynamic response performance of PEMFC. Lower oxygen supply will lead to "Oxygen Starvation" in PEMFC and reduce the output voltage of the stack. A higher oxygen supply will greatly increase the power consumed by the compressor and reduce the net power of PEMFC, which leads to "Oxygen Saturation" [5]. As an important component of the air supply subsystem, the compressor can ensure that the air supply subsystem can supply appropriate oxygen to the PEMFC stack [6]. Therefore, researchers often optimize oxygen supply and reduce compressor power consumption by quickly and accurately controlling the compressor to improve the dynamic response performance of PEMFC.

As the main parameters of the compressor, mass flow and intake pressure are often used as the control parameters of the compressor optimization algorithm. The oxygen

excess ratio (OER) is commonly used to describe the air mass flow provided by the air supply subsystem [7–9]. The OER is the ratio of the oxygen mass flow actually provided by the compressor to the fuel cell stack under the current request and the oxygen mass flow theoretically required by the electrochemical reaction. The research in references [10–12] shows that appropriately increasing the OER can avoid the stack reaction water blocking the gas channel and gas diffusion layer, and reduce the parasitic power consumption of the compressor, which is beneficial to improving the net power of PEMFC in general. At the same time, the inlet pressure provided by the air supply subsystem also has a very important impact on the voltage output characteristics of the stack. The inlet air pressure is usually characterized by the pressure ratio of the compressor, that is, the ratio of the outlet pressure of the compressor to the inlet pressure (atmospheric pressure) of the compressor [13]. A lower pressure ratio will affect the diffusion and supply of reactive gas in the stack, which makes it difficult for the stack to improve its voltage output performance and dynamic response performance. A higher pressure ratio will lead to the destruction of the proton exchange membrane (PEM) structure and the increase in compressor parasitic power, which will directly affect the improvement of the net power of FCS [14]. In references [15–17], researchers study the influence of stack pressure on the output power of FCS.

Aiming at the optimal control of the PEMFC air supply subsystem, researchers have proposed the control methods of OER [18]. Due to its simple structure and low cost, PID (Proportion Integration Differentiation) controller has become a more classical OER control algorithm. Zhao et al. proposed a fractional order PID controller based on a nonlinear observer to adjust the OER to the expected value. However, the PID control algorithm relies on engineering experience and lacks control accuracy [19]. Tang, X. et al. [20] reported an improved algorithm, coupled fuzzy logic and PID controller, and proposed an AFPID (Adaptive Fuzzy PID) control algorithm. However, the rules of fuzzy control are limited, and the control effect of OER still needs to be improved. MPC (Model Predictive Control) algorithm is also used in the optimal control of OER [21,22], but the MPC control model obtained by identifying and simplifying the controlled system is often difficult to obtain the optimal model accuracy and control effect.

However, the above studies did not fully consider the dynamic characteristics of the PEMFC system, nor how to obtain the optimal net output power of the PEMFC system. Therefore, this paper proposes an optimal control algorithm for the air supply subsystem to improve the net power output and dynamic response ability of the PEMFC system. Specifically, this paper has the following innovations: (1) The dynamic response model of the PEMFC system is established, and the optimal OER parameters with the highest net power of PEMFC under different load currents are determined. (2) A novel second-order active disturbance rejection control (2-ADRC) algorithm is proposed to make the OER parameters of PEMFC close to the optimal OER in real time, and at the same time, the two parameters of mass flow and pressure ratio of the air supply subsystem are considered comprehensively to make the compressor work in the high-efficiency zone.

This paper is organized as follows: In Section 2, the dynamic model of PEMFC is established and verified. In Section 3, a 2-ADRC algorithm is proposed and compared with PID and MPC algorithms, verifying the effectiveness and rationality of the 2-ADRC algorithm. Finally, the conclusions are drawn in Section 4.

2. PEMFC System Dynamic Model

The PEMFC system architecture adopted in this paper is shown in Figure 1. This paper mainly studies the control optimization of the air supply subsystem. Therefore, the air supply subsystem and PEMFC stack are described in detail in Figure 1.

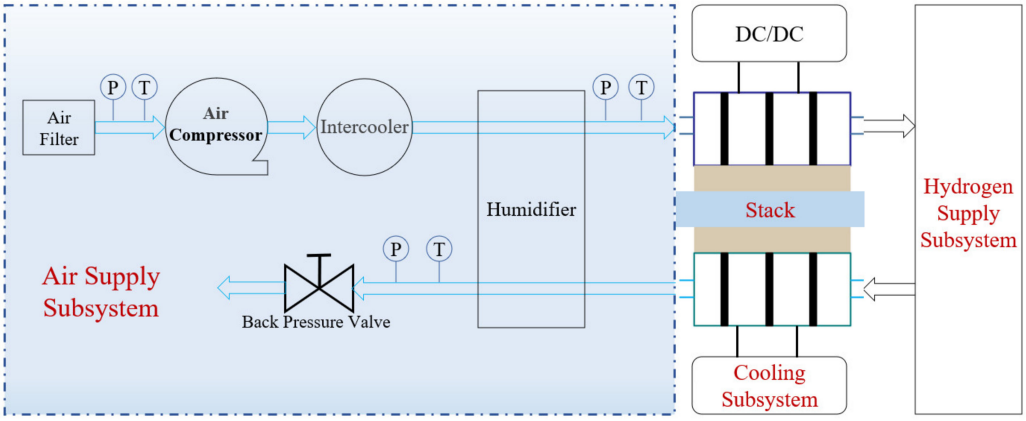

Figure 1. PEMFC system architecture.

The PEMFC dynamic model is established under the following assumptions: (1) gases conform to the ideal gas law and there is no interaction between gas molecules; (2) the water condensation, its saturation or two-phase flow in the cathode are not being considered; (3) the oxygen diffusion are ideal processes, and pressure changes will not affect the effective transport coefficients, mass transfer in the diffusing and catalytic layers.

2.1. Stack Model

2.1.1. Voltage Model

The output voltage V_{fc} of the fuel cell can be based on Srinivasan's empirical formula, and the following Formula (1) can be obtained [23]:

$$V_{fc} = E_{nenst} - V_{active} - V_{ohm} - V_{conc} \tag{1}$$

where E_{nenst} is the Nernst voltage, V_{active} is the activation polarization loss, V_{ohm} is the ohmic polarization loss and V_{conc} is the concentration polarization loss. Nernst voltage can be obtained from Formula (2):

$$E_{nenst} = 1.229 - 0.85 \times 10^{-3}(T_{st} - 298.15) + 4.3085 \times 10^{-5} T_{st}\left[\ln(p_{H_2}) + \frac{1}{2}\ln(p_{O_2})\right] \tag{2}$$

where T_{st} is the temperature of the fuel cell stack, P_{H_2} and P_{O_2} is the partial pressure of hydrogen and oxygen in the stack.

$$\begin{cases} V_{act} & = v_0 + v_a\left(1 - e_1^{-c_1 i_d}\right) \\ V_{ohm} & = i_d R_{ohm} = i_d \times \frac{t_m}{\sigma_m} \\ V_{conc} & = i_d\left(\frac{c_2 i_d}{i_{d\_\max}}\right)^{c_3} \end{cases} \tag{3}$$

where i_d is the current density, v_0 is the voltage drop when the current density is zero, v_a and c_1 are constants, and the values of v_0, v_a and c_1 can be obtained by nonlinear regression fitting of PEMFC stack test data. R_{ohm} is the equivalent resistance inside the stack, which can be obtained from the ratio of membrane thickness t_m to membrane conductivity σ_m. $i_{d\_\max}$ is the maximum current density of the stack, c_2 and c_3 are constants, closely related to the stack temperature and the partial pressure of the reaction gas.

$$\begin{cases} \sigma_m & = b_1 \exp(b_2(\frac{1}{303} - \frac{1}{T_{st}})) \\ b_1 & = (b_{11}\lambda_m - b_{12}) \end{cases} \tag{4}$$

where b_{11}, b_{12}, b_1 and b_2 are all empirical constants, and this paper estimates the ohm resistance in the stack according to the parameters in reference [24]. λ_m is the water content of the membrane.

2.1.2. Cathode Flow Model

According to the law of conservation of mass, the differential equations of oxygen, nitrogen and vapor on the cathode can be obtained as follows:

$$\frac{dm_{O_2,ca}}{dt} = W_{O_2,in,ca} - W_{O_2,out,ca} - W_{O_2,react,ca} \tag{5}$$

$$\frac{dm_{N_2,ca}}{dt} = W_{N_2,in,ca} - W_{N_2,out,ca} \tag{6}$$

$$\frac{dm_{v,ca}}{dt} = W_{v,in,ca} - W_{v,out,ca} + W_{v,gen,ca} + W_{v,mem} \tag{7}$$

where $m_{O_2,ca}$, $m_{N_2,ca}$ and $m_{v,ca}$ are the mass of oxygen, nitrogen and vapor at the cathode, respectively, $W_{O_2,in,ca}$, $W_{N_2,in,ca}$ and $W_{v,in,ca}$ are the mass flow of oxygen, nitrogen and vapor flowing into the cathode, respectively, $W_{O_2,out,ca}$, $W_{N_2,out,ca}$ and $W_{v,out,ca}$ are the mass flow of oxygen, nitrogen and vapor flowing out of the cathode, respectively, $W_{O_2,react,ca}$ is the mass flow of oxygen consumed by cathode reaction, $W_{v,gen,ca}$ is the mass flow of vapor generated by cathode reaction, $W_{v,mem}$ is the mass flow of vapor flowing to the anode through the PEM.

The mass flow of oxygen consumed and vapor generated in the cathode reaction can be expressed by the following formula:

$$W_{O_2,react,ca} = M_{O_2} \times \frac{I_{st}}{4F} \tag{8}$$

$$W_{v,gen,ca} = M_{H_2O} \times \frac{I_{st}}{2F} \tag{9}$$

where M_{O_2} and M_{H_2O} are the molar mass of oxygen and vapor, respectively, I_{st} is the stack current and F is the Faraday constant.

The mass flow of oxygen, nitrogen and water vapor flowing into the cathode can be expressed as:

$$W_{O_2,in,ca} = x_{O_2} \times W_{air,in,ca} \tag{10}$$

$$W_{N_2,in,ca} = \left(1 - x_{O_2}\right) \times W_{air,in,ca} \tag{11}$$

$$W_{v,in,ca} = W_{in,ca} - W_{O_2,in,ca} - W_{N_2,in,ca} \tag{12}$$

where $W_{air,in,ca}$ is the mass flow of dry air passing through the cathode, $W_{in,ca}$ is the total mass flow of gas passing through the cathode, and the relationship between the two is as follows:

$$W_{air,in,ca} = \frac{1}{1 + \omega_{in,ca}} W_{in,ca} \tag{13}$$

$$\omega_{in,ca} = \frac{p_{v,in,ca}}{p_{air,in,ca}} \frac{M_{H_2O}}{M_{air}} \tag{14}$$

where $\omega_{in,ca}$ is the cathode air humidity ratio, $p_{air,in,ca}$ is the cathode dry air partial pressure, $p_{v,in,ca}$ is the cathode vapor partial pressure, M_{air} is the molar mass of the dry air.

In Formulas (10) and (11), x_{O_2} is the mass fraction of oxygen in the dry air, which can be expressed as follows:

$$x_{O_2} = \frac{m_{O_2}}{m_{O_2} + m_{N_2}} \tag{15}$$

According to the General Gas Law, the partial pressure of each gas in the cathode can be expressed by the following formulas:

$$P_{i,ca} = \frac{m_{i,ca} R T_{st}}{V_{ca}} \tag{16}$$

$$P_{ca} = \frac{\left(m_{O_2} + m_{N_2} + m_v\right) R T_{st}}{V_{ca}} \tag{17}$$

where $i = O_2, N_2, v$, R are the ideal gas constant, V_{ca} is the volume of the stack cathode. There is a pressure drop between the cathode inlet and outlet, which is assumed to be uniform in this paper. Therefore, the cathode pressure can be considered as the average of the cathode inlet pressure $p_{in,ca}$ and cathode outlet pressure $p_{out,ca}$.

2.1.3. Anode Flow Model

The anode needs sufficient hydrogen supply during operation. Before hydrogen enters the stack, the gas pressure needs to be adjusted through the hydrogen injection valve to ensure the pressure difference between anode and cathode gas and protect the PEM. The anode side flow model can be obtained in a similar way to cathode side modeling:

$$\frac{dm_{H_2,an}}{dt} = W_{H_2,in,an} - W_{H_2,out,an} - W_{H_2,react,an} \tag{18}$$

$$\frac{dm_{v,an}}{dt} = W_{v,in,an} - W_{v,out,an} + W_{v,mem} \tag{19}$$

where $m_{H_2,an}$ and $m_{v,an}$ are the mass of hydrogen and vapor at the anode, respectively, $W_{H_2,in,an}$ and $W_{v,in,an}$ are the mass flow of hydrogen and vapor flowing into the anode, respectively, $W_{H_2,out,an}$ and $W_{v,out,an}$ are the mass flow of hydrogen and vapor flowing out of the anode, respectively, $W_{H_2,react,an}$ is the mass flow of hydrogen consumed by anode reaction, $W_{v,mem}$ is the mass flow of vapor flowing to the cathode through the PEM.

The hydrogen mass flow consumed in the anode reaction can be obtained by Formula (20):

$$W_{H_2,react,an} = M_{H_2} \times \frac{I_{st}}{2F} \tag{20}$$

where M_{H_2} is the molar mass of hydrogen.

The mass flow of hydrogen and vapor into the anode can be expressed as:

$$W_{H_2,in,an} = \frac{1}{1 + \omega_{in,an}} W_{in,an} \tag{21}$$

$$\omega_{in,an} = \frac{p_{v,in,an}}{p_{v,in,an} + p_{H_2,in,an}} \frac{M_{H_2O}}{M_{H_2} + M_{H_2O}} \tag{22}$$

$$W_{v,in,an} = W_{in,an} - W_{H_2,in,an} \tag{23}$$

where $\omega_{in,an}$ is the anode air humidity ratio, $W_{in,an}$ is the total mass flow of gas passing through the anode, $p_{H_2,in,an}$ is the partial pressure of hydrogen entering the anode, and $p_{v,in,an}$ is the partial pressure of vapor entering the anode.

According to the General Gas Law, the partial pressure of hydrogen and vapor in the anode can be expressed by the following formulas:

$$P_{i,an} = \frac{m_{i,an} R T_{st}}{V_{an}} \tag{24}$$

$$P_{an} = \frac{\left(m_{H_2} + m_v\right) R T_{st}}{V_{an}} \tag{25}$$

where $i = H_2, v$, V_{an} is the volume of stack anode.

2.1.4. Membrane Hydration Model

The model established in this paper is used to simulate the change of water content in PEM and the change of water mass flow through PEM. The mass flow of water through PEM $W_{v,mem}$ is mainly composed of two parts. The first part is electroosmosis, in which hydrogen ions at the anode drag water molecules to the cathode. The other part is the reverse diffusion phenomenon, due to the water concentration gradient between cathode and anode, some water molecules diffuse reversely from cathode to anode through PEM.

The water flow of electroosmosis $N_{v,osmotic}$ can be expressed as [25]:

$$N_{v,osmotic} = \frac{n_d i_d}{F} = \frac{(0.0029\lambda_m^2 + 0.05\lambda_m - 3.4 \times 10^{-19}) \times i_d}{F} \tag{26}$$

where the water content of the membrane λ_m is related to the average water activity of anode and cathode α_m, as shown in Formula (27).

$$\lambda_m = \begin{cases} 0.043 + 17.81\alpha_m - 39.85{\alpha_m}^2 + 36.0{\alpha_m}^3 & ,0 < \alpha_m \leq 1 \\ 14 + 1.4(\alpha_m - 1) & ,1 < \alpha_m \leq 3 \\ 16.8 & ,\alpha_m \geq 3 \end{cases} \tag{27}$$

The water flow of reverse diffusion $N_{v,diff}$ can be expressed as:

$$N_{v,diff} = D_w \frac{dc_v}{dy} = D_w \frac{C_{v,ca} - C_{v,an}}{t_m} \tag{28}$$

where C_v is the vapor concentration, y is approximately equal to the thickness of the membrane t_m, $C_{v,ca}$ and $C_{v,an}$ represent the concentration of cathode and anode vapor, respectively, which can be expressed by Formula (29):

$$c_{v,i} = \frac{\rho_{mem,dry}}{M_{mem,dry}} \lambda_m \tag{29}$$

where $i = ca, an$, $\rho_{mem,dry}$ is the density of dry membrane, $M_{mem,dry}$ is the dry membrane equivalent weight.

D_w in Formula (28) is the diffusion coefficient, which can be expressed by the following Formula (30):

$$D_w = \begin{cases} 10^{-6} \times \exp[2416(\frac{1}{303} - \frac{1}{T_{st}})] & , \quad \lambda_m < 2 \\ 10^{-6}[1 + 2(\lambda_m - 2)] \times \exp[2416(\frac{1}{303} - \frac{1}{T_{st}})] & , \quad 2 \leq \lambda_m \leq 3 \\ 10^{-6}[3 - 1.67(\lambda_m - 3)] \times \exp[2416(\frac{1}{303} - \frac{1}{T_{st}})] & , \quad 3 < \lambda_m < 4.5 \\ 1.25 \times 10^{-6} \times \exp[2416(\frac{1}{303} - \frac{1}{T_{st}})] & , \quad \lambda_m \geq 4.5 \end{cases} \tag{30}$$

Combined with the above two water transfer modes, the overall mass flow of water transfer can be obtained:

$$W_{v,mem} = \left(N_{v,osmotic} - N_{v,diff}\right) \times M_{H_2O} \times A_{fc} \times n = \left(\frac{n_d i_d}{F} - D_w \frac{C_{v,ca} - C_{v,an}}{t_m}\right) \times M_{H_2O} \times A_{fc} \times n \tag{31}$$

where A_{fc} is the reaction area of the single cell, and n is the number of cells in the stack.

2.2. Air Supply Subsystem Model

2.2.1. Compressor Model

The traditional compressor modeling and simulation is usually based on the static MAP of the compressor. Through the pressure ratio and speed of the compressor, the difference method is used to determine the air mass flow, but this method is not suitable for the dynamic simulation analysis of the compressor, so the nonlinear difference fitting

method is adopted in this paper. In the compressor model, the motor driving torque equations are used to simulate the dynamic characteristics, and the relevant Formulas are as follows [26]:

$$J_{cp}\frac{d\omega_{cp}}{dt} = (\tau_{cm} - \tau_{cp}) \tag{32}$$

where J_{cp} is the moment of inertia of the motor, ω_{cp} is the speed of the compressor, τ_{cm} is the driving torque of the motor, τ_{cp} is the resistance torque of the motor. The driving torque and resistance torque of the compressor drive motor are, respectively:

$$\begin{cases} \tau_{cm} & = \eta_{cm}\frac{k_t}{R_{cm}}(u_{cm} - k_v\omega_{cp}) \\ \tau_{cp} & = \frac{c_p}{\omega_{cp}}\frac{T_{atm}}{\eta_{cp}}\left[\left(\frac{p_{sm}}{p_{atm}}\right)^{\frac{\gamma-1}{\gamma}} - 1\right]W_{cp} \end{cases} \tag{33}$$

where k_t, R_{cm} and k_v are motor-related constants, η_{cm} is the mechanical efficiency of the motor, u_{cm} is the driving motor voltage, C_p is the specific heat of air, T_{atm} is the atmospheric temperature, η_{cp} is the compressor efficiency, p_{sm} is the pressure of the air supply manifold, which is related to the model of air supply manifold, p_{atm} is atmospheric pressure, γ is the specific heat ratio of air, W_{cp} is the mass flow of the compressor outlet gas.

2.2.2. Intercooler Model

Due to the high temperature of the air flowing out of the compressor, it must be cooled to protect the PEM. In this paper, it is assumed that the intercooler is an ideal intercooler, the change of temperature is not considered, and there is no pressure drop, so the flow in the intercooler does not change. At the same time, because the change of temperature will affect the humidity of the gas, the humidity leaving the intercooler ϕ_{cl} can be expressed by Formula (34):

$$\phi_{cl} = \frac{p_{cl}\phi_{atm}p_{sat}(T_{atm})}{p_{atm}p_{sat}(T_{cl})} = \frac{p_{sm}\phi_{atm}p_{sat}(T_{atm})}{p_{atm}p_{sat}(T_{cl})} \tag{34}$$

where p_{cl} is the air pressure in the intercooler, p_{sm} is the pressure in the supply manifold, and $p_{cl} = p_{sm}$. ϕ_{atm} is the atmospheric humidity, T_{cl} is the temperature of the air cooled by the intercooler, and p_{sat} is the saturation pressure of the vapor.

2.2.3. Supply Manifold Model

The supply manifold includes the total volume of the manifold connecting the compressor, intercooler, humidifier and other components with the stack [27]. For the mass m_{sm} and pressure p_{sm} in the supply manifold, the Formula (35) can be obtained from the Law of Conservation of Mass and the General Gas Law.

$$\begin{cases} \frac{dm_{sm}}{dt} & = W_{cp} - W_{sm,out} \\ \frac{dp_{sm}}{dt} & = \frac{\gamma R_a}{V_{sm}}(W_{cp}T_{cp} - W_{sm,out}T_{sm}) \end{cases} \tag{35}$$

where W_{cp} is the mass flow at the inlet of the supply manifold, which is equal to the mass flow at the outlet of the compressor, $W_{sm,out}$ is the outlet flow of the supply manifold, R_a is the air gas constant, V_{sm} is the volume of the supplied manifold. Due to the high temperature of the gas at the outlet of the compressor, the temperature will change when flowing through the supply manifold. T_{cp} is the compressor outlet gas temperature, and T_{sm} is the temperature of the gas inside the manifold.

Because the pressure difference between the supply manifold and the cathode inlet is relatively small, the outlet flow $W_{sm,out}$ of the supply manifold can be calculated by the linear function of the pressure difference between the supply manifold and the cathode inlet.

$$W_{sm,out} = k_{sm,out}(p_{sm} - p_{ca}) \tag{36}$$

where $k_{sm,out}$ is the supply manifold flow constant, and p_{ca} is the pressure at the cathode inlet.

2.2.4. Return Manifold Model

The air temperature in the return manifold is low, which can be assumed to be constant and equal to the outflow temperature of the cathode [28]. According to the Law of Conservation of Mass and the General Gas Law, the return manifold pressure p_{rm} can be obtained as follows:

$$\frac{dp_{rm}}{dt} = \frac{R_a T_{rm}}{V_{rm}}(W_{ca,out} - W_{rm,out}) \tag{37}$$

where $k_{sm,out}$ is the internal gas temperature of the return manifold, V_{rm} is the volume of the return manifold, $W_{ca,out}$ is the mass flow at the inlet of the return manifold, and $W_{rm,out}$ is the mass flow at the outlet of the return manifold, which can be expressed by Formula (38):

$$W_{rm,out} = \begin{cases} \frac{\alpha C_{D,rm} A_{T,rm} p_{rm}}{\sqrt{RT_{rm}}} \left(\frac{p_{atm}}{p_{rm}}\right)^{\frac{1}{\gamma}} \left\{ \frac{2\gamma}{\gamma-1} \left[1 - \left(\frac{p_{atm}}{p_{rm}}\right)^{\frac{\gamma-1}{\gamma}} \right] \right\}^{\frac{1}{2}}, \frac{p_{atm}}{p_{rm}} > \left(\frac{2}{\gamma+1}\right)^{\frac{\gamma}{\gamma-1}} \\ \frac{\alpha C_{D,rm} A_{T,rm} p_{rm}}{\sqrt{RT_{rm}}} (\gamma)^{\frac{1}{2}} \left(\frac{2}{\gamma+1}\right)^{\frac{\gamma+1}{2(\gamma-1)}}, \frac{p_{atm}}{p_{rm}} \le \left(\frac{2}{\gamma+1}\right)^{\frac{\gamma}{\gamma-1}} \end{cases} \tag{38}$$

where $C_{D,rm}$ is the flow coefficient of the return manifold, $A_{T,rm}$ is the area when the back pressure valve is fully open, and the value range α is 0~1, which is used to adjust the opening of the back pressure valve.

2.3. Model Validation

In order to verify the rationality of the PEMFC system model established in this paper, the main parameters in Table 1 are used to verify the output characteristics of the fuel cell stack, and the simulation verification results of the PEMFC system model shown in Figure 2 are obtained.

Table 1. Main parameters of PEMFC system.

Description	Parameters	Value
Structural parameters of the PEMFC	membrane thickness/cm	0.13
	active area of cells/cm^2	280
	cathode total volume/cm^3	0.01
Operating parameters of the PEMFC	number of cells	381
	temperature of the stack/K	353.15
	cathode air pressure/bar	1.78

There are always three kinds of polarization losses in the PEMFC stack. The activation polarization loss is the main factor at low current density, and the concentration polarization loss is the main factor at high current density, and because of the stack equivalent resistance, the ohmic polarization loss exists during the operation of the stack. The output characteristic curve of PEMFC is shown in Figure 2. The increasing current density inside the stack (see Figure 2a), the output voltage of the stack decreases, and the output power increases. Moreover, due to the influence of activation polarization loss and concentration polarization loss, the output voltage decreases significantly at the beginning and end of the output characteristic curve.

Figure 2b,c show the influence of stack temperature and cathode pressure on the output characteristic curve of a PEMFC single cell. In Figure 2b, with the increase in stack temperature, the reaction in the stack intensifies, and the output voltage of a single cell increases accordingly. In Figure 2c, with the increase in cathode pressure, the air supply in the reactor is timely, and the output voltage of a single cell is also increased accordingly. However, considering the stack materials, the stack internal sealing performance

and the power consumption of the accessory system, the stack temperature and cathode pressure cannot be increased without limit. The above analysis proves the rationality and effectiveness of the established PEMFC model.

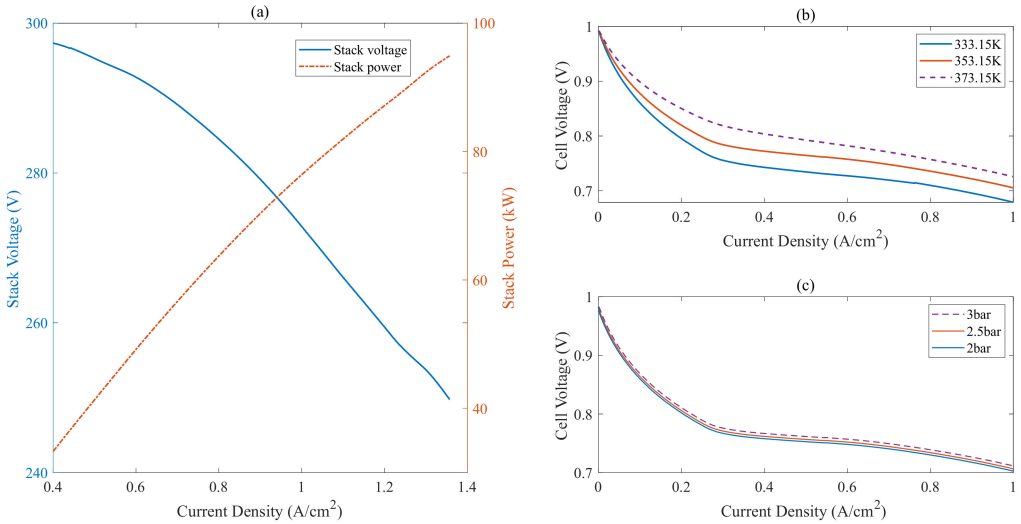

Figure 2. PEMFC model simulation and verification results: (**a**) Output characteristic curve; (**b**) Stack temperature; (**c**) Cathode pressure.

3. Optimal Control Algorithms of Air Supply Subsystem

3.1. Determination of Optimal Oxygen Excess Ratio

In the process of formulating the control algorithms for the air supply subsystem of the PEMFC, its dynamic characteristics should be considered. In other words, the power consumption of the compressor should be considered to optimize the net power and efficiency of PEMFC. The oxygen excess ratio represents the actual amount of air entering the stack, which has a great impact on the adequacy of the chemical reaction in the stack. By analyzing the test data of the fuel cell system, it is found that there exists an optimal oxygen excess ratio under a certain fixed current request, which maximizes the net power of the PEMFC system. The optimal oxygen excess ratio parameters of the PEMFC system are shown in Figure 3. Under the fixed current request of 180 A (see Figure 3a), when the oxygen excess ratio is 2.495, the net power of the fuel cell system reaches the maximum value of 47.30 kw. Therefore, 2.495 is the optimal oxygen excess ratio parameter of the PEMFC system at 180 A.

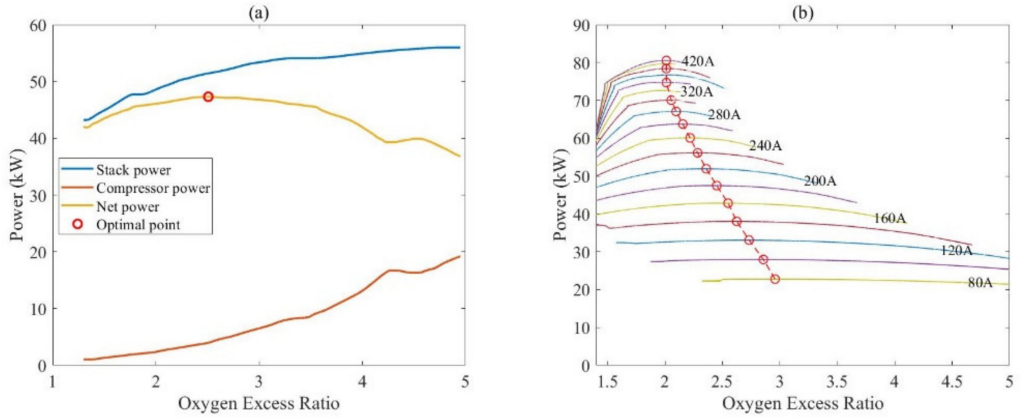

Figure 3. Optimal oxygen excess ratio parameters of the PEMFC system: (**a**) 180 A; (**b**) 180~240 A.

Under different load current requests, the oxygen excess ratio is changed by controlling the compressor driving motor voltage, and the curve of the change of PEMFC net power

with oxygen excess ratio can be obtained, and then find the optimal oxygen excess ratio under the fixed current request, as shown in Figure 3b. The load current is controlled to change from 80 A to 420 A (see Figure 3b), the step is 20 A, and the oxygen excess ratio is controlled to change between 1.5 and 3.5. The variation curve of the PEMFC net power with the oxygen excess ratio under each fixed current request is obtained. Under different load current requests, there exists an optimal oxygen excess ratio, which maximizes the PEMFC net power. The optimal oxygen excess ratio parameters of the PEMFC system are shown in Table 2.

Table 2. Optimal oxygen excess ratio parameters of the PEMFC system.

Load Current Request	Optimal Oxygen Excess Ratio	Load Current Request	Optimal Oxygen Excess Ratio
80 A	2.958	200 A	2.387
100 A	2.856	220 A	2.284
120 A	2.732	240 A	2.218
140 A	2.624	260 A	2.180
160 A	2.549	280 A	2.097
180 A	2.495	300 A	2.054

3.2. Air Supply Subsystem Optimization Control Algorithms

In order to achieve better dynamic response and higher net power and efficiency of PEMFC, it is necessary to ensure that the actual oxygen excess ratio of PEMFC in the working process is close to the optimal oxygen excess ratio shown in Table 2. In order to improve the optimal control effect of the PEMFC air supply subsystem, a second-order active disturbance rejection control (2-ADRC) algorithm is proposed in this paper. At the same time, in order to verify the rationality and effectiveness of the 2-ADRC algorithm, it is compared with the PID algorithm and MPC algorithm. The control structure is shown in Figure 4 in this paper. Moreover, Figure 5a is the simulation condition (load current change condition) of the PID algorithm, MPC algorithm and 2-ADRC algorithm, and Figure 5b is the curve of optimal oxygen excess ratio variation under load current variation, which can be called the reference optimal oxygen excess ratio.

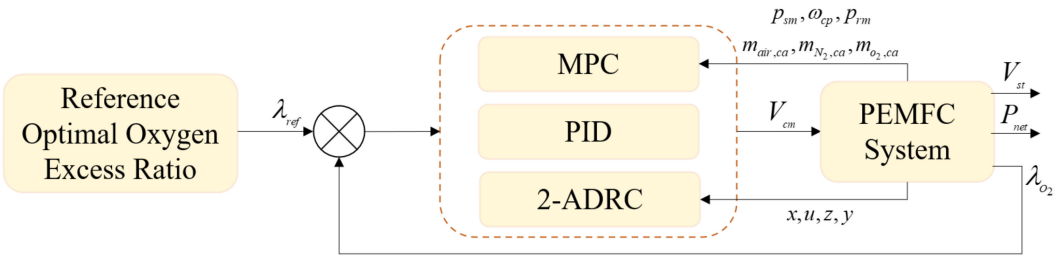

Figure 4. Control structure of air supply subsystem.

3.2.1. PID Algorithm

The PID algorithm is a classical control algorithm for oxygen excess ratio in the PEMFC air supply subsystem [29]. The PID algorithm designed in this paper takes the error between the optimal oxygen excess ratio λ_{ref} and the actual oxygen excess ratio λ_{O_2} as the PID controller input, and the control voltage v_{cm} of the compressor driving motor is the PID controller output. By changing the voltage of the driving motor, the compressor speed can be further adjusted to change the airflow into the stack. The PID controller is designed as PI type, and P = 85, I = 3200. The simulation results of the PID control algorithm designed in this paper are shown in Figure 6.

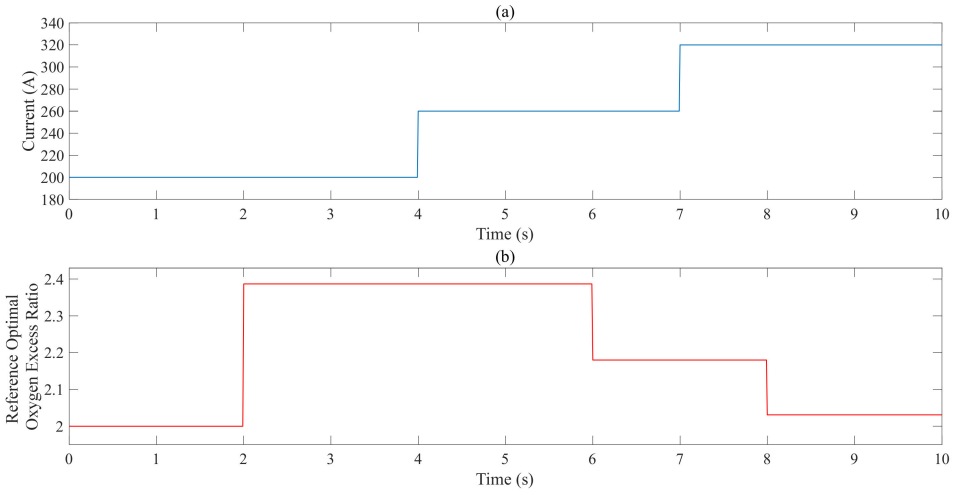

Figure 5. The simulation condition: (**a**) Load current change condition; (**b**) Reference optimal oxygen excess ratio.

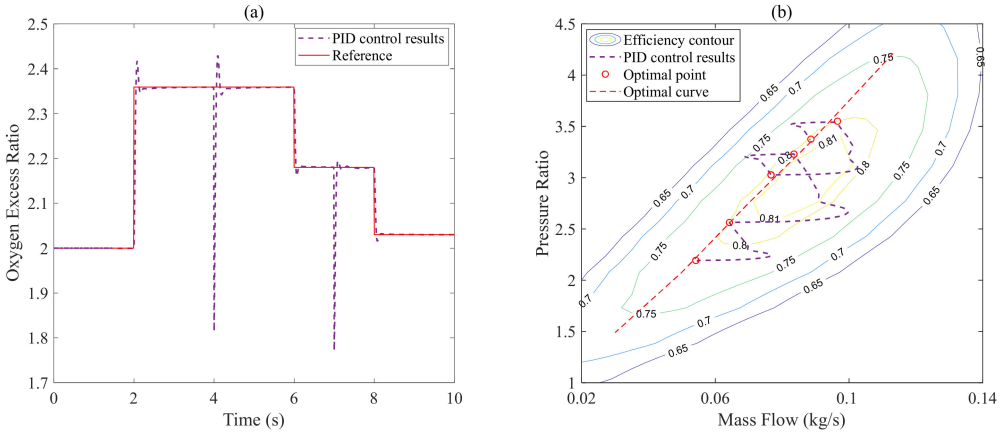

Figure 6. PID algorithm simulation results: (**a**) Oxygen excess ratio following curve; (**b**) Compressor mass flow and pressure ratio curve.

In Figure 5a, the load current changes step at 4 s and 7 s, and in Figure 5b, the optimal oxygen excess ratio changes step at 2 s, 6 s and 8 s. Therefore, at 2 s, 4 s, 6 s, 7 s and 8 s in Figure 6a, the actual oxygen excess ratio changes, and the oxygen excess ratio can be adjusted to the target value under the regulation of the PID control algorithm, but there is a certain amount of overshoot. In the overshoot condition, the compressor will deviate from the stable operating point under the fixed current request. In Figure 6b, the compressor mass flow and pressure ratio curve deviates from the set optimal working curve, and at the same time, due to the overshoot of the oxygen excess ratio during the control process, the compressor efficiency will decrease.

3.2.2. MPC Algorithm

The Simulink model of the PEMFC established in this paper is a complex nonlinear system model. In this paper, the LTI linear toolbox of MATLAB is used to linearize the model and obtain the linearized state-space model of the PEMFC system, which is used as the predictive model of the MPC algorithm. In the specific MPC algorithm design process, the compressor drive motor voltage v_{cm} is selected as the algorithm control variable, and the oxygen excess ratio λ_{O_2} is selected as the algorithm output variable [30], and the air supply manifold pressure p_{sm}, the compressor speed ω_{cp}, the return manifold pressure p_{rm},

the cathode air mass $m_{air,ca}$, the cathode nitrogen mass $m_{N_2,ca}$ and the cathode oxygen mass $m_{O_2,ca}$ are used as algorithm state variables. The following formulas can be obtained.

$$\begin{cases} \dot{x} &= Ax + Bu \\ y &= Cx \end{cases} \tag{39}$$

where u is the control variable, y is the output variable, and x is the state variable, which can be expressed as:

$$\begin{cases} u &= v_{cm} \\ y &= \lambda_{o_2} \\ x &= [p_{sm}, \omega_{cp}, p_{rm}, m_{air,ca}, m_{N_2,ca}, m_{o_2,ca}]^T \end{cases} \tag{40}$$

The load current 260 A, the compressor drive motor voltage 226 V, and the oxygen excess ratio 2.18 are selected as the equilibrium operating points of the linear MPC model. After the model is balanced and stable, the values of state variables are shown in Table 3.

Table 3. Values of state variables in MPC algorithm.

p_{sm}	ω_{cp}	p_{rm}	$m_{air,ca}$	$m_{N_2,ca}$	$m_{O_2,ca}$
3.003×10^5	1.696×10^4	2.439×10^5	9.818×10^{-4}	1.938×10^{-2}	0.971×10^{-3}

At the same time, the eigenvalues of matrix A in Formula (39) can be obtained: $\mathrm{eig(A)} = [-20.43 \ -23.6 \ -1.09 \ -4.13 \ -98.55 \ -119.36]$. The simulation results of the MPC algorithm designed in this paper are shown in Figure 7.

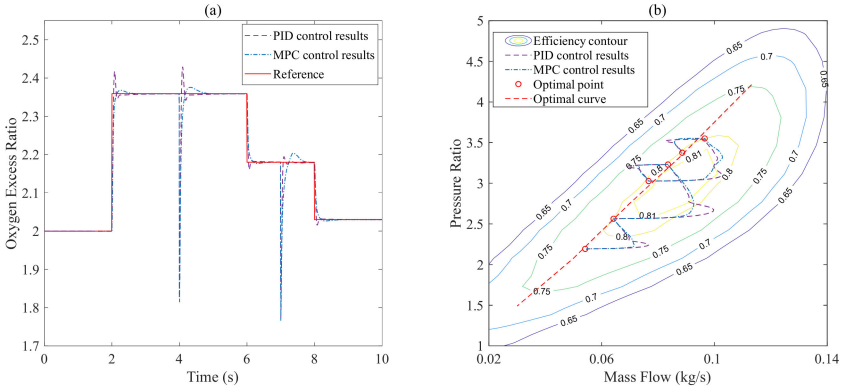

Figure 7. MPC algorithm simulation results: (**a**) oxygen excess ratio following curve; (**b**) Compressor mass flow and pressure ratio curve.

In Figure 7a, with the change of the optimal reference value of the oxygen excess ratio at 2 s and 6 s and the step change of the current request at 4 s, the oxygen excess ratio can quickly reach the optimal reference value with almost no overshoot under the adjustment of the MPC algorithm. However, when the load current changes step at 7 s, the oxygen excess ratio cannot quickly adjust to the optimal reference value under the control of the MPC algorithm, and there is a certain degree of overshoot. The prediction model used by the MPC controller in this paper is a linearized model obtained under a fixed current operating point. Therefore, this linearized model is not suitable for controlling the optimization of the oxygen excess ratio under various currents of the complex PEMFC system. In Figure 7b, the compressor mass flow and pressure ratio curve deviates from the set optimal working curve, but it is better than the control result of the PID algorithm.

3.2.3. 2-ADRC Algorithm

Under the step load current request, the compressor drive motor input voltage is selected as the input variable, and the oxygen excess ratio is selected as the output variable to obtain the PEMFC sample data. Then, using the identification toolbox of MATLAB for parameter identification, the sample time interval is 0.01 s, and the relationship between the input voltage of the compressor drive motor of the air supply subsystem and the excess oxygen ratio can be obtained.

$$\ddot{y} = -1027\dot{y} - 3.007y + 3.586u + 0.01521\dot{u} \tag{41}$$

where u is the compressor drive motor voltage, which is used as the algorithm input, and y is the oxygen excess ratio, which is used as the algorithm output. Furthermore, the Formula (41) can be transformed into the Formula (42).

$$\begin{array}{ll} \ddot{y} & = -1027\dot{y} - 3.007y + 0.01521\dot{u} + (3.586 - b_0)u + b_0u \\ & = f + b_0u \end{array} \tag{42}$$

where f is regarded as the "total disturbance" of the controlled system, including modeled and external disturbances.

In the specific design of the 2-ADRC algorithm, reducing the influence of the total disturbance is of great significance to the algorithm's control effect and the estimator $\hat{f}$ of total disturbance f is introduced in the design of 2-ADRC. In order to obtain the $\hat{f}$ correctly, an extended state observer is designed. According to Formula (41), the system state space equation can be obtained.

$$\begin{cases} \dot{x} & = Ax + Bu + Eh \\ y & = Cz \end{cases} \Leftrightarrow \begin{cases} \dot{x}_1 & = x_2 \\ \dot{x}_2 & = x_3 + b_0u \\ \dot{x}_3 & = h \\ y & = x_1 \end{cases} \tag{43}$$

where $x_3 = f$ and $h = \dot{f}$, which extends the f to a new state variable that can be observed by the state observer and A, B, C and E are represented as follows.

$$A = \begin{bmatrix} 0 & 1 & 0 \\ 0 & 0 & 1 \\ 0 & 0 & 0 \end{bmatrix}, B = \begin{bmatrix} 0 \\ b_0 \\ 0 \end{bmatrix}, C = \begin{bmatrix} 1 & 0 & 0 \end{bmatrix}, E = \begin{bmatrix} 0 \\ 0 \\ 1 \end{bmatrix} \tag{44}$$

Then, the state space equation of the second-order LESO extended state observer can be shown as follows:

$$\begin{cases} \dot{z} & = Az + Bu + L(y - \hat{y}) \\ \hat{y} & = Cz \end{cases} \tag{45}$$

$$\begin{cases} \dot{z}_1 & = \beta_1(y - z_1) + z_2 \\ \dot{z}_2 & = \beta_2(y - z_1) + b_0u + z_3 \\ \dot{z}_3 & = \beta_3(y - z_1) \end{cases} \tag{46}$$

$$\dot{z} = \begin{bmatrix} -\beta_1 & 1 & 0 \\ -\beta_2 & 0 & 1 \\ -\beta_3 & 0 & 0 \end{bmatrix} z + \begin{bmatrix} 0 & \beta_1 \\ b_0 & \beta_2 \\ 0 & \beta_3 \end{bmatrix} \begin{bmatrix} u \\ y \end{bmatrix} \tag{47}$$

where $L = \begin{bmatrix} \beta_1 & \beta_2 & \beta_3 \end{bmatrix}^T$ and $z_3 = \hat{f}$. The algorithm input u can be converted to $u = (-z_3 + u_0)/b_0$, and combined with Formula (42), while ignoring the influence of z_3, the following Formula (48) can be obtained.

$$\ddot{y} = (f - z_3) + u_0 \approx u_0 \tag{48}$$

For the simplified model, the PD-type controller is adopted to control the error, and the following Formula (49) can be obtained.

$$u(t) = K_p e(t) + \frac{de(t)}{dt} \Rightarrow u_0 = k_p(r - z_1) - k_d z_2 \tag{49}$$

where r is the reference and the closed-loop transfer function of 2-ADRC can be obtained in Formula (50), which characterizes the relationship between input voltage of compressor driving motor and oxygen excess ratio of air supply subsystem. The simulation results of the 2-ADRC algorithm designed in this paper are shown in Figure 8.

$$G_{cl} = \frac{y(s)}{r(s)} = \frac{k_p}{s^2 + k_d s + k_p} \tag{50}$$

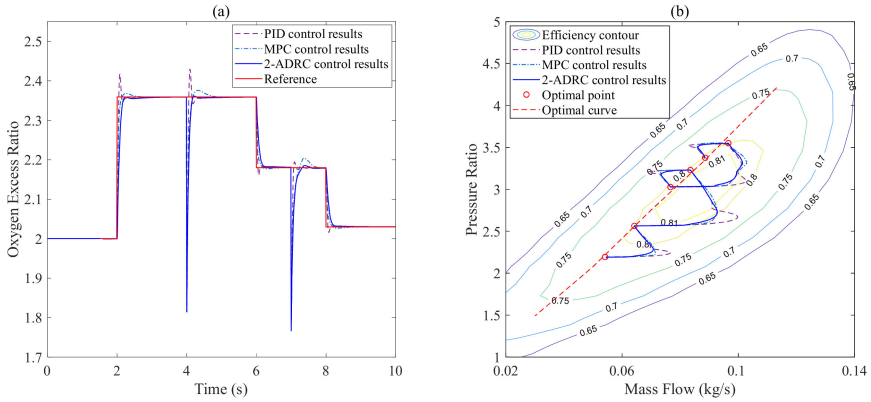

Figure 8. 2-ADRC algorithm simulation results: (**a**) Oxygen excess ratio following curve; (**b**) Compressor mass flow and pressure ratio curve.

In Figure 8a, when the load current request and the reference oxygen excess ratio change, the PEMFC air supply subsystem can quickly adjust the oxygen excess ratio to reach the optimal reference value. Compared with the PID algorithm and MPC algorithm, the 2-ADRC algorithm can quickly adjust the oxygen excess ratio to the optimal reference value without overshoot and achieve a better control effect of the oxygen excess ratio in the PEMFC air supply subsystem. In Figure 8b, when adjusting the oxygen excess ratio of the air supply subsystem, the compressor speed will be quickly adjusted to improve the air mass flow into the FCS. Therefore, the power consumption of the compressor will rise instantaneously, and the mass flow and pressure ratio curve of the compressor will also deviate from the set optimal working curve. Compared with the PID algorithm and MPC algorithm, the 2-ADRC algorithm can make the compressor work in the high-efficiency zone.

In order to verify the effectiveness of the proposed 2-ADRC algorithm more comprehensively, the power and efficiency curves of the PEMFC system under the control of the PID algorithm, MPC algorithm and 2-ADRC algorithm are also obtained. The stack power, compressor power and net power of the PEMFC system are shown in Figure 9, and the PEMFC system efficiency and compressor efficiency are shown in Figure 10.

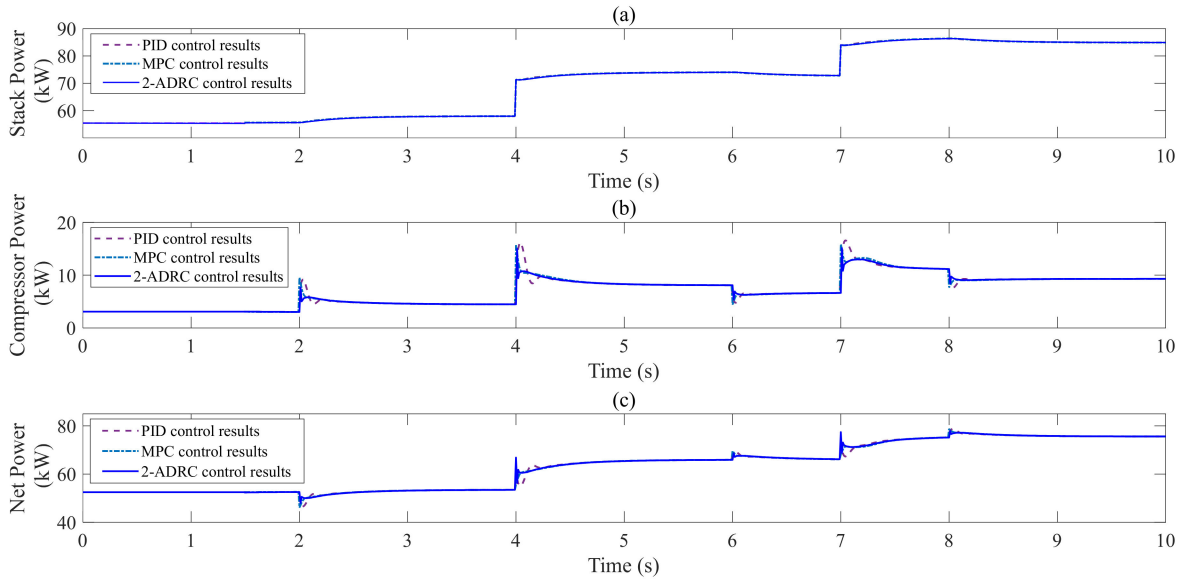

Figure 9. Power simulation results: (**a**) Stack power; (**b**) Compressor power; (**c**) Net power.

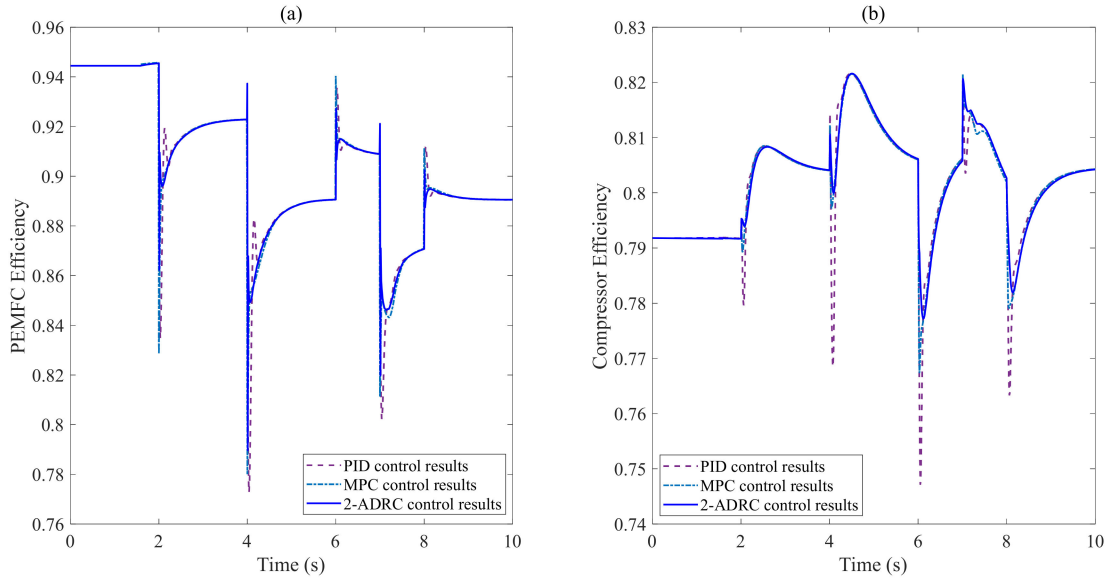

Figure 10. Efficiency simulation results: (**a**) PEMFC efficiency; (**b**) Compressor efficiency.

In Figure 9a, the PID algorithm, MPC algorithm and 2-ADRC algorithm can ensure the stack output power meets the requirements. In Figure 9b, the power consumption of the compressor under the control of the PID algorithm is significantly higher than that of the MPC algorithm and the 2-ADRC algorithm, and the power consumption of the compressor under the control of the MPC algorithm is also slightly higher than that of the 2-ADRC algorithm. In Figure 9c, the net power of the PEMFC system controlled by the PID algorithm is significantly lower than that of the MPC algorithm and 2-ADRC algorithm, and the net power of the PEMFC system controlled by the MPC algorithm is also slightly lower than the 2-adrc algorithm. In Figure 10a, the efficiency of the PEMFC system controlled by the PID algorithm is significantly lower than the MPC algorithm and 2-ADRC algorithm, and the efficiency of the PEMFC system controlled by the MPC algorithm is also slightly lower than the 2-ADRC algorithm. Furthermore, similar conclusions can be obtained from the simulation results of compressor efficiency in Figure 10b. Based on the above discussion, it can be concluded that the 2-ADRC algorithm proposed in this paper is superior to the PID algorithm and MPC algorithm. The 2-ADRC algorithm can make the

compressor work in the high-efficiency zone and improve the net power and efficiency of the PEMFC system.

4. Conclusions

This paper analyzes the dynamic characteristics of the PEMFC system, and the dynamic Simulink model of the PEMFC system is established and verified. In order to propose the optimal control algorithms for the PEMFC air supply subsystem, the OER parameters with the highest net power of PEMFC under different load currents are determined, and the OER parameters are regarded as the control target of the algorithms. A 2-ADRC algorithm is further proposed to optimize air supply subsystem control of the PEMFC system, and the 2-ADRC algorithm can quickly adjust the OER of the air supply subsystem to reach the optimal reference value and make the actual OER parameters close to the optimal OER in real time. Compared with the PID algorithm and MPC algorithm, the 2-ADRC algorithm can comprehensively consider the two parameters of mass flow and pressure ratio to make the compressor work in the high-efficiency zone and improve the net power and efficiency of the PEMFC system.

Author Contributions: Conceived the structure and research direction of the paper, P.W. and Y.M.; wrote the paper and provided algorithms, Y.M. and Y.G.; software, data curation and project administration, J.L.; formal analysis and validation, Y.G. and Y.Z.; validation and writing—original draft preparation, Y.M., Y.G. and D.M. All authors have read and agreed to the published version of the manuscript.

Funding: The work was supported by the National Key R&D Program of China (grant no. 2021YFB2500700).

Institutional Review Board Statement: Not applicable.

Informed Consent Statement: Not applicable.

Data Availability Statement: The data may be available after request from corresponding authors.

Conflicts of Interest: The authors declare no conflict of interest.

References

1. Kendall, M. Fuel cell development for New Energy Vehicles (NEVs) and clean air in China. *Prog. Nat. Sci. Mater. Int.* **2018**, *28*, 113–120. [CrossRef]
2. Ahmadi, P.; Torabi, S.H.; Afsaneh, H.; Sadegheih, Y.; Ganjehsarabi, H.; Ashjaee, M. The effects of driving patterns and PEM fuel cell degradation on the lifecycle assessment of hydrogen fuel cell vehicles. *Int. J. Hydrogen Energy* **2020**, *45*, 3595–3608. [CrossRef]
3. Wang, G.J.; Yu, Y.; Liu, H.; Gong, C.L.; Wen, S.; Wang, X.H.; Tu, Z.K. Progress on design and development of polymer electrolyte membrane fuel cell systems for vehicle applications: A review. *Fuel Process. Technol.* **2018**, *179*, 203–228. [CrossRef]
4. Yuan, H.; Dai, H.F.; Wei, X.Z.; Ming, P.W. Model-based observers for internal states estimation and control of proton exchange membrane fuel cell system: A review. *J. Power Sources* **2020**, *468*, 228376. [CrossRef]
5. Liu, J.X.; Gao, Y.B.; Su, X.J.; Wack, M.; Wu, L.G. Disturbance-observer-based control for air management of PEM fuel cell systems via sliding mode technique. *IEEE Trans. Control Syst. Technol.* **2019**, *27*, 1129–1138. [CrossRef]
6. Li, J.W.; Yu, T. Intelligent controller based on distributed deep reinforcement learning for PEMFC air supply system. *IEEE Access* **2021**, *9*, 7496–7507. [CrossRef]
7. Pukrushpan, J.T.; Stefanopoulou, A.G.; Peng, H. Control of fuel cell breathing. *IEEE Control Syst. Mag.* **2004**, *24*, 30–46.
8. Chen, J.; Liu, Z.Y.; Wang, F.; Ouyang, Q.; Su, H.Y. Optima Oxygen Excess Ratio Control for PEM Fuel Cells. *IEEE Trans. Control Syst. Technol.* **2018**, *26*, 1711–1721. [CrossRef]
9. Hou, J.B.; Yang, M.; Ke, C.C.; Zhang, J.L. Control logics and strategies for air supply in PEM fuel cell engines. *Appl. Energy* **2020**, *269*, 115059. [CrossRef]
10. Kim, B.M.; Choi, Y.H.; Yoo, S.J. Adaptive control of proton exchange membrane fuel cell air supply systems with asymmetric oxygen excess ratio constraints. *IEEE Access* **2020**, *8*, 5537–5549. [CrossRef]
11. Zhang, H.K.; Wang, Y.F.; Wang, D.H.; Wang, Y.L. Adaptive robust control of oxygen excess ratio for PEMFC system based on type-2 fuzzy logic system. *Inf. Sci.* **2020**, *511*, 1–17. [CrossRef]
12. Tian, Y.; Zou, Q.; Liu, J.Q.; Han, J. Novel hybrid control scheme of a proton exchange membrane fuel cell air supply system. *Energy Technol.* **2022**, *10*, 2100906. [CrossRef]
13. Luna, J.; Usai, E.; Husar, A.; Serra, M. Enhancing the efficiency and lifetime of a proton exchange membrane fuel cell using nonlinear model-predictive control with nonlinear observation. *IEEE Trans. Ind. Electron.* **2017**, *64*, 6649–6659. [CrossRef]

14. Hoeflinger, J.; Hofmann, P. Air mass flow and pressure optimisation of a PEM fuel cell range extender system. *Int. J. Hydrogen Energy* **2020**, *45*, 29246–29258. [CrossRef]
15. Tafaoli-Masoule, M.; Shakeri, M.; Esmaili, Q.; Bahrami, A. PEM fuel cell modeling and pressure investigation. *Energy Sources Part A* **2011**, *33*, 2291–2302. [CrossRef]
16. Ogungbemi, E.; Wilberforce, T.; Ijaodola, O.; Thompson, J.; Olabi, A.G. Review of operating condition, design parameters and material properties for proton exchange membrane fuel cells. *Int. J. Energy Res.* **2020**, *45*, 1227–1245. [CrossRef]
17. Ahmadi, N.; Dadvand, A.; Rezazadeh, S.; Mirzaee, I. Analysis of the operating pressure and GDL geometrical configuration effect on PEM fuel cell performance. *J. Braz. Soc. Mech. Sci. Eng.* **2016**, *38*, 2311–2325. [CrossRef]
18. Daud, W.; Rosli, R.; Majlan, E.; Hamid, S.; Mohamed, R.; Husaini, T. PEM fuel cell system control: A review. *Renew. Energy* **2017**, *113*, 620–638. [CrossRef]
19. Zhao, D.D.; Li, F.; Ma, R.; Zhao, G.S.; Huangfu, Y.G. An unknown input nonlinear observer based fractional order PID control of fuel cell air supply system. *IEEE Trans. Ind. Appl.* **2021**, *56*, 5523–5532. [CrossRef]
20. Tang, X.; Wang, C.S.; Hu, Y.K.; Liu, Z.J.; Li, F.L. Adaptive fuzzy PID based on granular function for proton exchange membrane fuel cell oxygen excess ratio control. *Energies* **2021**, *14*, 1140. [CrossRef]
21. Ouyang, Q.; Chen, J.; Wang, F.; Su, H.Y. Nonlinear MPC controller design for AIR supply of PEM fuel cell based power systems. *Asian J. Control* **2017**, *19*, 929–940. [CrossRef]
22. Danzer, M.A.; Wittmann, S.J.; Hofer, E.P. Prevention of fuel cell starvation by model predictive control of pressure, excess ratio, and current. *J. Power Sources* **2009**, *190*, 86–91. [CrossRef]
23. Srinivasan, S.; Ticianelli, E.A.; Derouin, C.R.; Redondo, A. Advances in solid polymer electrolyte fuel cell technology with low platinum loading electrodes. *J. Power Sources* **1988**, *22*, 359–375. [CrossRef]
24. Springer, T.; Rockward, R.; Zawodzinski, T.; Gottesfeld, S. Model for polymer electrolyte fuel cell operation on reformate feed—Effects of CO, H_2 dilution, and high fuel utilization. *J. Electrochem. Soc.* **2001**, *148*, A11–A23. [CrossRef]
25. Rowe, A.; Li, X.G. Mathematical modeling of proton exchange membrane fuel cells. *J. Power Sources* **2001**, *102*, 82–96. [CrossRef]
26. Sun, L.; Shen, J.; Hua, Q.S.; Lee, K.Y. Data-driven oxygen excess ratio control for proton exchange membrane fuel cell. *Appl. Energy* **2018**, *231*, 866–875. [CrossRef]
27. Hames, Y.; Kaya, K.; Baltacioglu, E.; Turksoy, A. Analysis of the control strategies for fuel saving in the hydrogen fuel cell vehicles. *Int. J. Hydrogen Energy* **2018**, *43*, 10810–10821. [CrossRef]
28. Biyikoglu, A. Review of proton exchange membrane fuel cell models. *Int. J. Hydrogen Energy* **2005**, *30*, 1181–1212. [CrossRef]
29. Benchouia, N.E.; Derghal, A.; Mahmah, B.; Madi, B.; Khochemane, L.; Aoul, E.H. An Adaptive Fuzzy Logic Controller (AFLC) for PEMFC fuel cell. *Int. J. Hydrogen Energy* **2015**, *40*, 13806–13819. [CrossRef]
30. Vrlic, M.; Ritzberger, D.; Jakubek, S. Safe and efficient polymer electrolyte membrane fuel cell control using successive linearization based model predictive control validated on real vehicle data. *Energies* **2020**, *13*, 5353. [CrossRef]